SOFT ROBOTICS
Volume 00, Number 00, 2024

DOI: 10.1089/soro.2024.0063

SoRo
Soft Robotics

ORIGINAL ARTICLE

Automatic Design Framework of Dielectric Elastomer Actuators: Neural Network-Based Real-Time Simulation, Genetic Algorithm-Based Electrode Optimization, and Experimental Verification

Zijian Qin,[1,2,*] Jieji Ren,[1,2,*] Feifei Chen,[1,2] Jiang Zou,[1,2] and Guoying Gu[1,2]

Abstract

Dielectric elastomer actuators (DEAs) enable to create soft robots with fast response speed and high-energy density, but the fast optimization design of DEAs still remains elusive because of their continuous electromechanical deformation and high-dimensional design space. Existing approaches usually involve repeating and vast finite element calculation during the optimization process, leading to low efficiency and time consuming. The advance of deep learning has shown the potential to accelerate the optimization process, but the high-dimensional design space leads to challenge on the accuracy and generality of the deep learning model. In this work, we propose a deep learning-based automatic design framework for DEAs, capable of rapidly generating high-dimensional distributed electrode patterns based on different design objects. This framework is developed as follows: (1) a dataset construction strategy combining with a finite element model is developed to optimize the data distribution within the high-dimensional design space; (2) a neural network-embedded physical information is designed and trained to achieve accurate prediction of the continuous deformation within 0.011*s*; and (3) a genetic algorithm with the neural network is proposed to automatically and rapidly optimize the electrode pattern of DEAs based on various design objects. To verify the effectiveness, a series of case studies (including maximum displacement, specific displacement, multiplicity of solutions, multiple degree-of-freedom actuations, and complex actuations) has been conducted. Both simulation results and experimental data demonstrate that our design framework can automatically design the electrode pattern within 2 min and obviously improve the performance of DEAs. This work proposes a deep learning-based design approach with automatic and rapid property, thereby paving the way for broader applications of DEAs.

Keywords: dielectric elastomer actuators (DEAs), neural network-embedded physical information, genetic algorithm-based optimization design, continuous deformation, distributed electric field

[1]State Key Laboratory of Mechanical System and Vibration, Shanghai Jiao Tong University, Shanghai, China.
[2]Robotics Institute School of Mechanical Engineering, Shanghai Jiao Tong University, Shanghai, China.
*These authors contributed equally to this work and should be considered co-first authors.

Introduction

Soft robots, capable of safely interacting with humans and manipulating objects in unstructured environments, represent a burgeoning technology in the field of robotics. Those bioinspired mechanical features of soft robots mainly come from the muscle-like materials (known as artificial muscles), such as shape memory polymers,[1–6] pneumatic and fluid actuators,[7–11] and dielectric elastomer actuators (DEAs).[12–15] Due to the advantages of electric actuation, fast response speed, high-energy density, and ease of integration, DEAs have been widely used to develop advanced soft robots.

In general, DEAs mainly consist of a dielectric elastomer membrane coated with compliant electrodes on both sides. When a high voltage is applied, the Maxwell stress between the electrodes squeezes the membrane, leading to expansion in area and decrease in thickness. Based on this working principle, DEAs with various configurations have been proposed to generate different actuations, such as elongation,[16–18] bending,[19–22] and contracting.[23,24] Furthermore, there are a lot of mechanical achievements in the design of dielectric elastomer-actuated soft robots, such as the flying robot,[25–27] deep sea swimming robot,[28,29] wall-climbing robot,[30–32] soft pocket pump,[33] and wearable haptic device,[34–37] becoming an important trend in the development of soft robots. As the application of DEAs is emerging, the automatic design of DEAs is increasingly being desired. However, due to the nonlinear electromechanical coupling, continuous deformation, and high-dimensional design space, the automatic design of DEAs faces huge challenge.

Most of the previous works mainly focus on establishing physical models[38–43] to explain the experimental phenomena (such as large deformation, mechanical instability, electric breakdown, and viscoelasticity) of DEAs. However, it is difficult to obtain the inverse analytical models for these physical models, limiting their application in the design of DEAs. As a result, most existing DEAs mainly adopt an intuitive or empirical design paradigm for prescribed object, limiting their output potential for larger actuation capability. To overcome the above drawback, some gradient-descent optimization approach-embedded finite element method have been proposed to improve the performance of DEAs, such as pairs of Bezier curve,[44,45] fat Bezier curve,[46] 0–1 layout,[47] the level set-based topology optimization method,[48] and the Solid Isotropic Material with Penalization method.[45,49] In general, those approaches usually involve three steps: (1) calculating the continuous deformation under series of random electrode patterns based on finite element model (FEM); (2) calculating the gradient of the object function; and (3) updating the electrode patterns based on gradient-descent topology optimization methods and repeating the above process. By taking the advantage of gradient-descent iteration, the electrode patterns would be updating during the optimization process. However, vast finite element calculations of the optimization process lead to low efficiency and time consuming for one single prescribed target. Moreover, FEM could not achieve the convergence results as the design parameters increase, limiting their applications for designing DEAs with high-dimensional design space.

The advance of deep learning is capable of describing complex nonlinear mechanical systems with high accuracy and efficiency,[50,51] showing potential application in solving the optimization problems, such as mechanical design[52,53] and chemical synthesis.[54,55] Recently, some deep learning-based design methods have been proposed in the field of soft robotics. For example, Bertoldi *et al.* have proposed a deep learning-based inverse design approach that can obtain an optimal 2D elastomer membrane and the inflation pressure for target 3D shape. Renaud *et al.* have adopted the convolutional neural network and the Bezier curve-based genetic algorithm (GA) to optimize the inner structure of pneumatic actuators.[56] Li et al. have proposed a graph neural network-based methods to optimize the supporting frame of DEA with a minimum energy structure.[57] Different from those finite element-based optimization approaches, deep learning-based design method usually starts from constructing a proper dataset and train a neural network model to predict the continuous deformation under arbitrary design parameters, achieving fast optimization design. In general, the key of deep learning-based design methods depends on the accuracy and generality of neural network model trained on constructed dataset. Usually, the dataset consists of randomly generated design parameters and the continuous deformation calculated by FEM. To construct the dataset for training a deformation prediction model, a common approach is to randomly sample the design space (which is the electrode pattern). However, due to the high-dimensional design space of DEAs, randomly selecting the electrode patterns to construct the deformation dataset exits bias, as the increase of random parameters of the high-dimensional design space leads to the small deformation due to the fragmental electrodes. While the large deformation is usually demanded for the applications of DEAs. And the dataset is difficult to cover the whole deformation space of DEAs with randomly sampling of high-dimensional design space. As a result, the accuracy and generality of the deep learning model may deteriorate, limiting their applications for high-dimensional design spaces. To date, existing deep learning-based methods mainly focus on optimizing a small number of design parameters. How to rapidly design the distributed electrodes of DEAs still remains elusive.

In this work, we propose a deep learning-based design framework to design the distributed electric field of DEAs fast and automatically. To this end, we first adopt the neo-Hookean constitutive model to describe the nonlinear electromechanical effect of dielectric elastomer material and establish a membrane element through a user-defined material model (UMAT) in ABQUAS. Then, a dataset evaluation method and dataset construction strategy are developed to optimize the electrode sampling for the high-dimensional design space. Furthermore, a neural network is trained on the dataset-embedded physical information to describe the relationship between distributed electric field and continuous deformation of DEAs. Lastly, by using the fast deformation prediction neural network as a surrogate model, a GA is adopted to automatically optimize the distributed electric field (Supplementary Movie S1). To validate the effectiveness, we employ the framework to automatically optimize the distributed electric field according to different design objects, such as specific displacement and maximum displacement of single point or multiple points. Both the calculated results (FEM and Neural Network predicted) and the

experimental data demonstrate that: (1) the Neural Network (NN) model trained on the constructed dataset can predict the deformations of DEAs precisely compared with the FEM results ($RMSE \leq 0.065$) (*RMSE* represents root-mean square error), showing the generality of the constructed dataset; (2) the NN model can realize the continuous modeling of DEAs with high-dimensional design space and can precisely predict the continuous deformation of DEAs within $0.011s$; (3) by taking the advantage of the rapid prediction, the framework can reduce the computational load and accelerate the DEAs optimization design process by three orders (about $120s$) based on various design objects (Supplementary Movie S2); and (4) the framework can achieve the multiple inverse designs of DEAs with high-dimensional design space, in which multiple solutions may widely exist for the same design object. This work would contribute to rapidly and automatically design DEAs with high performance and high-dimensional design spaces, accelerating the practical applications of DEAs.

Method

Working principle of the design framework

Figure 1 shows the working principle of the automatic design framework for DEAs based on different design objects. In general, a planar DEA mainly consists of a prestretched dielectric elastomer membrane (made of acrylic, 3M VHB 4910, thickness of 1.0 mm size of 50 mm × 50 mm, prestretch of 3.0×3.0) that is supported by a stiff frame (acrylic, thickness of 3.0 mm). Carbon grease (MG846-80G), working as a compliant electrode, is utilized to coat on both sides of the dielectric elastomer membrane (see Supplementary Fig. S1 for more details about the fabrication process of the planar DEAs). The electrode divides the dielectric elastomer membrane into two regions: active and passive region. Under excitation voltage, the output displacement of the end effector relies on both the active deformation of the active region and the passive deformation of the passive region, as shown in Figure 1a. However, due to the nonlinear electromechanical effect, continuous deformation, and high-dimensional design space, it is difficult to establish a design model to optimize the electrode pattern directly. To date, automatic design of electrode pattern still faces challenges. To solve this problem, our design framework (Fig. 1b) mainly involves three steps:

1. A neo-Hookean FEM is first established to obtain the continuous deformation under distributed electrodes. In our work, we focus on the static responses of DEAs instead of dynamic responses. Then, we adopt a neo-Hookean constitutive model without considering the viscosity of the material (see Supplementary Data S1 and Supplementary Fig. S2 for more details about the development of the FEM). Moreover, a dataset evaluation method and dataset construction strategy are developed to optimize the electrode sampling for high-dimensional design space, paving the way for training a deep learning model.
2. Based on the dataset, a neural network-embedded physical information is designed and trained, which can accurately predict the continuous deformation within $0.011s$ with $RMSE \leq 0.065$ under distributed

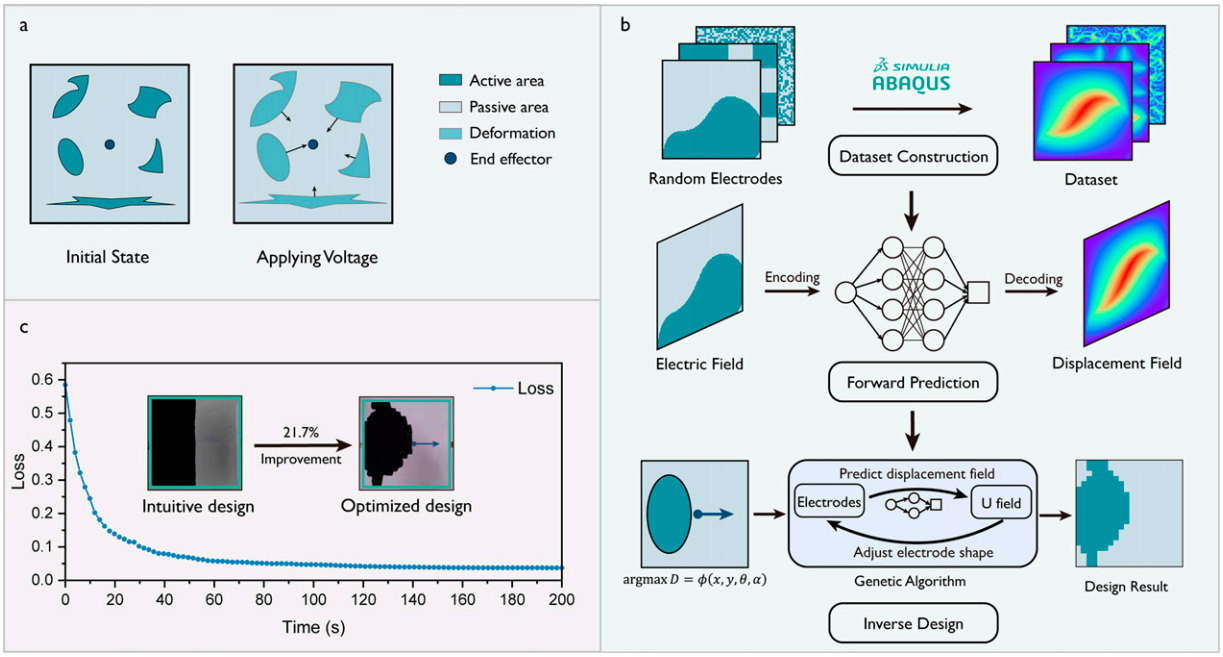

FIG. 1. Automatic design framework for DEAs. **(a)** Working principle of the planar DEAs. **(b)** Illustration of the workflow of the automatic design framework. First, we employ finite element method to construct and optimize the dataset. Then, based on the dataset, a neural network model is trained to rapidly predict the continuous deformation of DEAs under random electrode patterns. Finally, based on the neural network model, a GA is developed to achieve automatic design of DEAs according to desired performance. **(c)** Displacement field of DEAs with fragmental and continuous electrode patterns. **(d)** One example of the automatic designed DEAs, whose performance is improved by 21.7%, compared with the intuitive design. DEAs, dielectric elastomer actuators; GA, genetic algorithm.

electrodes. Compared with the FEM, the neural network can accelerate the simulation process by three orders, achieving real-time simulation.

3. The trained neural network is working as the surrogate model and a GA-based optimization method is adopted to automatically design distributed electrodes of DEAs. For proof-of-concept testing, a series of case studies (including maximum displacement, specific displacement, multiplicity of solutions, multiple degree-of-freedom actuations, and complex actuations) have been conducted. Both simulation results and experimental data demonstrate that our design framework can automatically design the electrode pattern within 2 min. Supplementary Movie S1 shows one example of the design process of the planar DEA. It can be observed that it only takes about 120 s to obtain the desired electrode pattern. Compared with existing design methods (Supplementary Table S1), our design framework can accelerate the design process by three orders. In addition, with the designed electrode pattern, the displacement of the central point is 21.7% larger than that of intuitive design (Fig. 1d), validating the effectiveness of our automatic design framework.

Based on the above working principle of our design framework, the key is to establish an accurate surrogate model. To this end, we first need to construct a proper dataset that satisfies the following conditions: (1) its deformation distribution should cover the deformation space of the planar DEA under any electrode pattern and (2) the size of the dataset should be affordable. However, due to the high-dimensional design space of the distributed electrodes, the deformation space is difficult to figure out. Increasing the size of the dataset may contribute to enlarging the deformation space of the dataset, but it leads to time-consuming calculation. In this work, we propose a dataset evaluation and augmentation approach to construct the dataset.

Dataset construction

In general, the dataset consists of a series of distributed electrode patterns and corresponding continuous deformations. The first step is to generate distributed electrode patterns. To this end, the dielectric elastomer membrane is meshed into small squares, and we use "0" and "1" to represent without and with electrodes of each small square, respectively. It should be noted that the performance of the planar DEAs relies on the total area of the electrode. Without loss of generality, we first set the total area of the electrode pattern as half of the dielectric elastomer membrane and expand it to changing area. In addition, the prediction accuracy of the complex deformation field can be improved by reducing the size of the small square, but it will enlarge the design space and lead to fabrication problems. Therefore, this work adopts 1.0 mm as the size of the square, and the dielectric elastomer membrane is meshed into 50×50 units. As a result, there are 2^{2500} permutation and combination of electrodes, and the design space is too large to be fully enumerated. Therefore, we need a strategy to generate the proper dataset. We would like to mention that the prediction space of the neural network model usually relies on the deformation space of the dataset. In the meantime, the predicted results of the neural network model also are biased toward high probability area in the dataset. As the random parameters of the high-dimensional design spaces increase, the electrode patterns tend to be fragmental. The fragmental electrodes lead to the small deformation while the large deformation is usually demanded for the applications of DEAs. Therefore, the dataset is difficult to randomly sample the whole deformation space with uniform sampling of the design space. To maximize the deformation space and remove the data bias of the dataset, we first propose a data evaluation method.

Specifically, we first define the range of the maximum displacement under arbitrary electrode as the deformation space. Based on our experience, the deformation space of planar DEAs is selected as $[0, 2.5]$ mm. Then, the deformation space is divided into uniform M segments ($M = 100$ in this work). For any electrode pattern $\phi_i (i = 1, 2, ..., n)$, the max displacement d_i of the FEM results can be denoted as:

$$d_i = \max_i f(\phi_i) \tag{1}$$

where $f(\phi_i)$ is the continuous deformation distribution under the electrode pattern ϕ_i. Then, the probability density of the dataset is defined as:

$$g\left(\frac{2j}{M}\right) = \frac{n_j\left(\frac{2(j-1)}{M} \le d < \frac{2j}{M}\right)}{n} \tag{2}$$

where n_j represents the number of d_j that satisfies $\left(\frac{2(j-1)}{M} \le d\_\mathrm{j} < \frac{2j}{M}, j = 1, 2, ..., M\right)$ in the dataset, n represents the total number in the dataset.

Based on the above evaluation method, the dataset is constructed by the following four steps. The first step is to randomly generate electrode patterns. We adopt a random algorithm (randomly select 1250 units out of 2500 and set as 1) to generate 10,000 electrodes patterns (called small grid) and calculate the continuous deformation through the FEM. Based on the dataset with small grid electrode patterns, we can obtain the probability density of the small grid-based dataset (Fig. 2a). It can be seen that most of the data are concentrated on the small deformation area. Based on the dataset, a neural network model is also trained, which is working as the surrogate model for optimizing the design of planar DEAs. However, for the designed planar DEA, its maximum deformation predicted by the surrogate model is much smaller than that of the FEM with same electrode pattern (see Supplementary Fig. S5 for more details about the surrogate model based on the random electrode-based dataset). It is worth noting that the prediction RMSE of fragmental electrode patterns increases for the model trained without the small grid-based dataset predicted. The main reason depends on the fact that the small grid-based dataset is concentrated on the small deformation area due to fragmental electrodes. As a result, the trained surrogate model cannot predict large deformation.

To reduce the fragmentation, the second step is to enlarge the size of the unit (called large grid-based dataset). We adopt another nine kinds of size to mesh the dielectric elastomer membrane, including 2×2, 3×3,

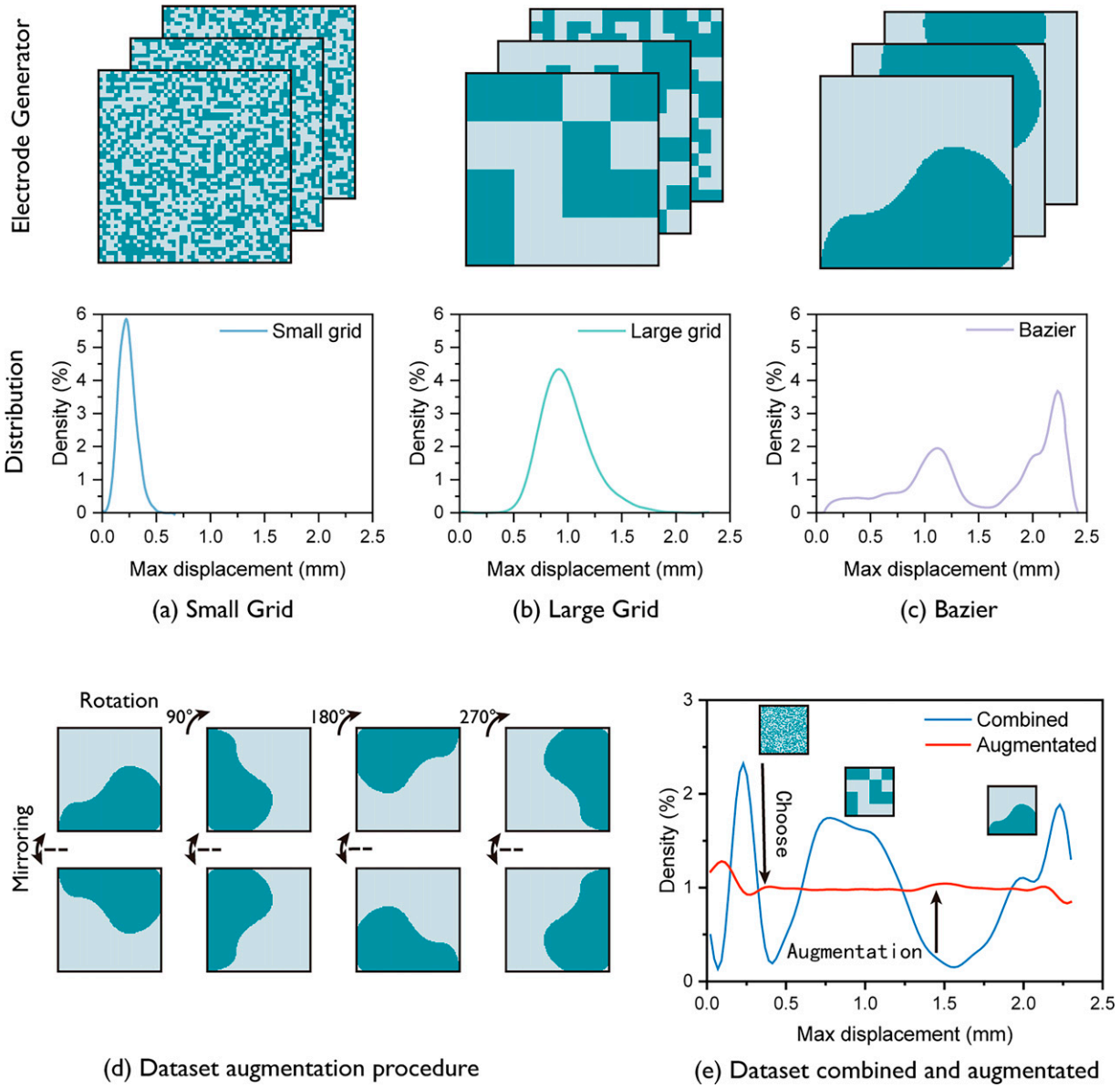

FIG. 2. Construction of the dataset. **(a)** Dataset based on the small grid electrode pattern. **(b)** Dataset based on the large grid electrode pattern. **(c)** Dataset based on the Bezier curve electrode pattern. **(d)** Dataset is augmented by rotation and mirroring. **(e)** The data distribution of augmented dataset.

4×4, 5×5, 6×6, 7×7, 8×8, 9×9, and 10×10. For the 2×2 and 3×3, the sample size is small, so all of them are added into the large grid-based dataset. For the rest seven kinds of size, the sample size is very large. Therefore, we randomly select about a thousand electrode patterns for each mesh unit. Furthermore, we analyze the probability density distribution of the large grid-based dataset (Fig. 2b). It demonstrates that by enlarging the size of the unit, the output displacement is improved. However, on the one hand, the maximum displacement in the dataset concentrates around 1 mm, which will lead to prejudice for training surrogate model. On the other hand, the large grid causes nonsmooth edge of the electrode pattern.

To overcome the above drawback, the third step is to adopt a Bezier curve method to generate continuous electrodes. We choose two arbitrary points along the edge and middle point as the through points, then two hyperparameters are introduced to generate four control points of the cubic Bezier curve. By randomly sampling the two arbitrary points and two hyperparameters, we obtain 10,000 Bezier curve-based electrode patterns. The probability density distribution of the Bezier curve-based dataset (Fig. 2c) demonstrates that it can significantly expand the maximum displacement distribution of the dataset. Based on the above three steps, we obtain three datasets with three different probability density distributions. Furthermore, we use them to construct a bigger dataset and analyze its probability density distribution, shown in Figure 2e. It can be observed that the displacement in the dataset can cover different displacement levels, including small, middle, and large deformation. However, as the distribution is still ununiform, the sample size under different deformation is unbalanced and the

trained surrogate model will tend to be high probability area. To further improve the generality of the dataset, the fourth step is to augment the dataset. Due to the geometric symmetry property of planar DEA, the displacement field of the electrode after transformation (rotation or mirroring) is the same transformation of previous displacement field, paving a way to augment the data. As shown in Figure 2d and Supplementary Fig. S3d, the process of data augmentation include the following three steps: (1) evaluate the maximum displacement distribution of all the electrodes in the original dataset; (2) split the electrodes by the uniform distribution curve; (3) for the electrode with a large sample size (maximum displacement above the uniform distribution), we calculate how many times it is larger than the uniform distribution (e.g., n times) and then randomly sample the electrodes with a ratio of $\frac{1}{n}$; and (4) for the electrode with a small sample size (maximum displacement beneath the uniform distribution), we first augment the electrode by eight times with rotation and mirroring,[58] then repeat steps (2) and (3) once.

Finally, we construct a dataset with physical information that consists of $10k$ electrode patterns with a uniform max displacement distribution (Fig. 2e, and details on the dataset construct methods are shown in Supplementary Fig. S3.). To further illustrate the contribution of these electrode generation methods and dataset construction approaches, we trained the NN model on various datasets and compare the predicted deformations with FEM results. As shown in Supplementary Fig. S5, the RMSE of the trained model based on the augmented dataset is better, shows the accuracy of the NN model. Based on the above dataset construction strategy and the augmented dataset, we next train a surrogate model to rapidly predict the continuous deformation under any distributed electrodes.

Neural network-embedded physical information-based surrogate model

With the physical prior knowledge of DEAs, we build a specialized convolutional neural network to model the continuous deformation of the planar DEA under distributed electric field.

Design of the neural network. To describe the relationship between the distributed electric field and the continuous deformation, we define it as a nonlinear mapping problem. The input is distributed electric field S and the output is the displacement field U. The nonlinear mapping can be expressed as:

$$f_\theta(S) = U \tag{3}$$

where θ is the parameters of neural network f. To accurately predict the displacement field from distributed electric filed, we design a convolutional neural network with physical information, which can (1) extract the special features from distributed electrode patterns; (2) transform them into high-dimensional feature space; (3) bridge the gap between special spatial features and geometrical displacement features; and (4) reconstruct the displacement field. Figure 3a shows the framework of neural network that consists of encoder module, nonlinear mapping, decoder module, and multiscale supervision.

Encoder module is the feature extraction part, which is used to extract spatial features from electrode pattern distribution. To sufficiently extract local and global information, we utilize a five-layer sequential neural network. Considering that DEA has mechanical and electrical continuity, and strong interactions in adjacent electric nodes, we take large kernels in the early layer to increase the receptive fields and extract features, which can depict the spatial correlations, and fuse local information to generate effective features. Each layer can perform nonlinear transformation. Five-layer neural network can effectively extract local and global features from raw data and mapping them into high-dimensional embedding space. The bottleneck layers are used to map extracted spatial features to high-dimensional displacement feature space for successive decoding and reconstruction process.

Decoder module is the reconstruction part, which is utilized to decode the high-dimensional features into displacement field. Here, we utilize three convolutional neural network layers, which gradually enlarges the spatial resolution and reduces the feature dimension, and finally reconstructs the displacement field. Considering the displacement on X and Y directions are strongly coupled and implied in the spatial features of electric pattern, we build two parallel branches to reconstruct horizontal displacement simultaneously (Supplementary Fig. S4). Furthermore, to increase efficiency and stability of the training process, we add an assistive branch to help the neural network converge. The branch takes $1/2X$ as a reconstruct target and can guide network modeling process. Due to the symmetrical data, $1/2X$ branch can act as a $1/2Y$ branch in some extend and only design one 1/2 branch for network efficiency. In the whole network, 1/2 branch is acting as coarse scale, which can reconstruct global and coarse displacement, while full-scale branch can further provide details and high-resolution displacement field. With multiscale branch structure and corresponding supervisions, the training process would be more stable and converge fast, as well as higher performance.

Loss function of the neural network. The target of the proposed network is estimating the accurate displacement under distributed electric field. To introduce the physical mechanism into our predicting model, we design the loss function to guide the network leaning process and minimize the output error. We first choose the L1 smooth loss to make the output displacement fiddle close to the ground truth. L1 smooth loss can provide stable loss sign for the network without big gradient backpropagation. The maximum displacement output represents the motion capacity of DEAs, which is important to constrain the noise and outlier that may affect the training process. Thus, we introduce the maximum displacement error into loss function that is used to constrain the error and abnormal points. Besides, a hyperparameter λ is introduced to adjust their contribution in training processes. We utilize backpropagation to transfer the loss value to each layer and update the parameters to minimize the prediction error between $f(S)$ and U. The loss function can be expressed as follows:

$$L_i\big(U\,|\,f(S)\big) = \|U_i - f(S_i)\|_1 + \lambda \max \|U_i - f(S_i)\|_1 \tag{4}$$

Based on the above loss function, the neural network is trained to predict the continuous deformation field. We train five prediction models based on the datasets in Figure 2,

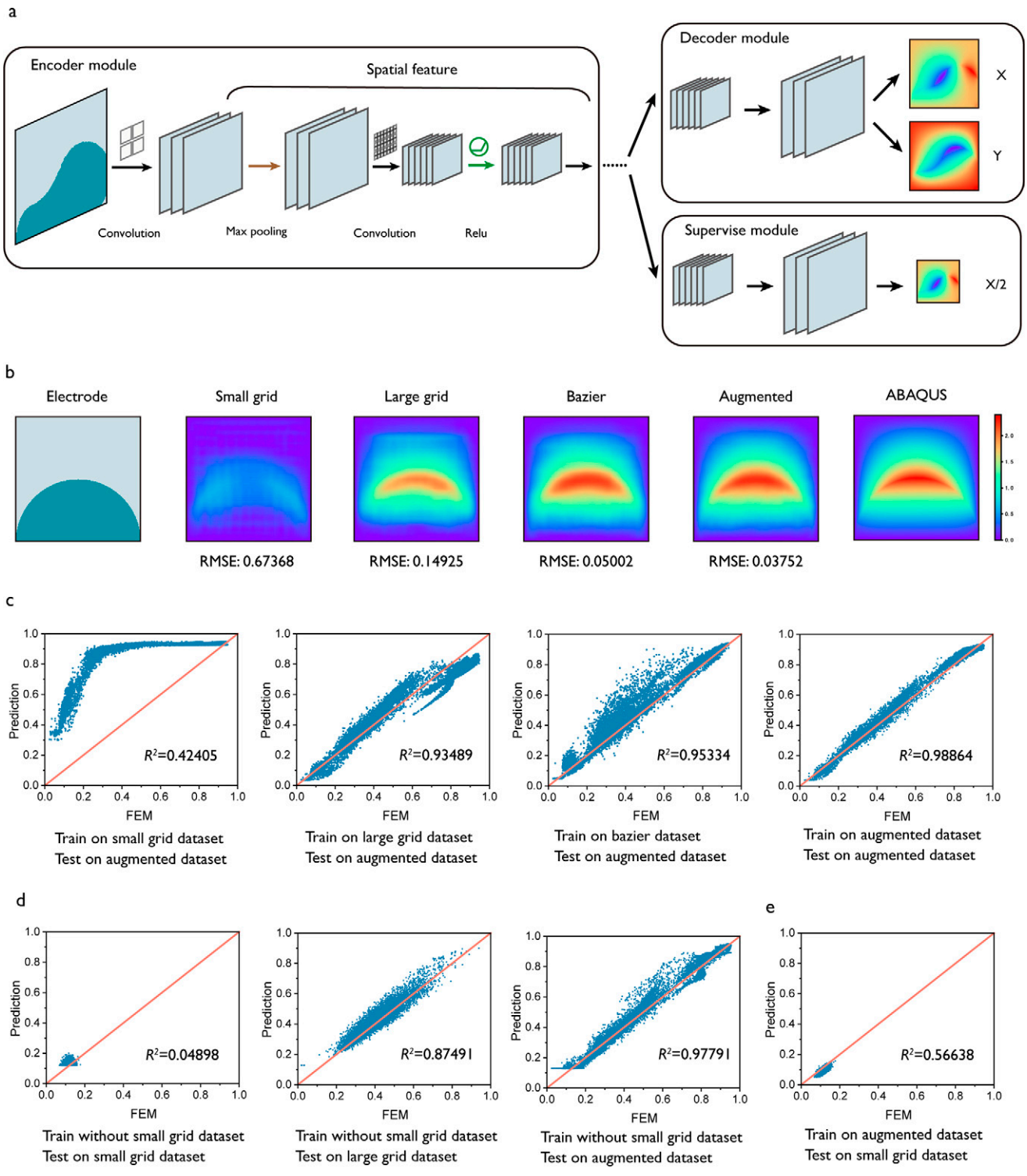

FIG. 3. Design and validation of the neural network. **(a)** Structure of the neural network, including the encoder module, decoder module, and supervise module. **(b)** Predicted displacement field by neural network models trained on small grid, large grid, Bezier, augmented dataset, and FEM result by ABAQUS of a half circle electrode pattern. RMSE is calculated to denote the accuracy of these neural network models. **(c)** Comparison of predicted maximum displacement of augmented dataset between models trained on small grid, large grid, Bezier, and augmented dataset. R^2 is calculated to represent the goodness of fit between predicted model and FEM. **(d)** Comparison of predicted normalized maximum displacement of small grid, large grid, and augmented dataset by the model trained without small grid electrode patterns. **(e)** Predicted normalized maximum displacement of small grid dataset by the model trained on augmented dataset. FEM, finite element model; RMSE, root-mean square error.

including small grid, large grid, Bezier, augmented, and without small grid datasets. Figure 3b shows one example of the finite element analysis of DEAs and the prediction result based on models trained on five datasets. It can be seen that with the augmented dataset, the surrogate model can precisely predict the continuous deformation. Compared with the FEM simulation results, the RMSE is <0.06, which is considered an acceptable prediction error. Furthermore, we adopt three electrode patterns to validate the effectiveness of those surrogate models (Fig. 3b and Supplementary Fig. S5). Based on the simulation results, the maximum displacement of each electrode pattern of the surrogate model is plotted as a function of that of the FEM. Linear coefficient of determination R^2 is calculated to represent the linearity of predicted models and PV (peak to valley) of the error (FEM result minus predicted field) is calculated to present the bias of models. As shown in Figure 3c, the small grid-based surrogate model cannot accurately predict the relationship between continuous deformations and distributed electrode patterns. By enlarging the grid and introducing Bezier curve-based electrode pattern, the accuracy of the surrogate model is improved, but there is still obvious bias. By augmenting the dataset, the performance is significantly enhanced, verifying the effectiveness of our dataset construction approach.

We then trained a model without small grid dataset and test the predicted maximum displacement of each electrode pattern of the dataset. The results in Figure 3d show that the model trained without small grid dataset cannot predict the deformation in small scale of deformation, while the model trained by the augmented dataset could predict the deformation during all deformation space (Fig. 3e). We then predict the displacement field of several electrode pattern on various datasets (Supplementary Fig. S5). The model trained without small grid dataset has twice as much error PV as the model trained on augmented dataset when the maximum displacement of input electrode pattern is at a small level. In addition, for the neural network-based surrogate model, it only takes $0.011s$ to obtain the predicted results. Compared with FEM, it can accelerate the simulation process by three orders, paving the way for rapidly designing the electrode patterns of DEAs. In the following section, we adopt the augmented dataset-based surrogate model to automatically design DEAs.

GA-based inverse design

Based on the surrogate model, many kinds of optimization approaches can be used. Considering the serious nonlinearity of DEAs and high-dimensional design space, we adopt a GA to optimize the distributed electrodes of the planar DEAs in this work.

To optimize the electrode pattern, we first need to define a design object. Although the DEAs can generate continuous deformations, we usually only care about the performance of a few points. Without loss of generality, the design object is defined as maximum displacement of specific points, which can be expressed as:

$$\arg\max D = \phi(x, y, \theta, \alpha) \tag{5}$$

where x, y, θ represent the coordinate and motion direction of the target point. ϕ is the excitation voltage. D is the displacement of the target point, and α is the area fraction of the electrodes. Furthermore, we define a loss function (Lagrangian function) as:

$$F_i(D \mid \phi(x, y, \theta)) = 1 - \frac{\|D_x^i \cos\theta + D_y^i \sin\theta\|_1}{\|D^i\|_2} + \lambda\|\alpha_i - \alpha\|_1 \tag{6}$$

where α_i is the area fraction of each electrode pattern, λ is a Lagrangian operator, and α is the target area fraction. D_x^i and D_y^i are the components of the target point displacement along the x and y direction. The $\frac{\|D_x^i \cos\theta + D_y^i \sin\theta\|_1}{\|D^i\|_2}$ represents the normalized in desired direction.

With the loss function, we employ the GA to achieve the inverse design of DEAs, as shown in Figure 4a. To this end, we first mesh the dielectric elastomer membrane into 20×20 units and use "0" and "1" to present the unit without and with electrode, respectively. Then, the electrode pattern is coded as chromosomes. Lastly, the optimization process mainly involves the following steps (Supplementary Fig. S6 and Supplementary Movie S1): (1) 1000 random electrode patterns is generated, which is working as the initial population; (2) the continuous deformations of each initial population are predicted based on the surrogate model; (3) the value of the loss function is calculated based on the displacement field and sorted from smallest to largest; (4) the populations with smallest 2% of loss functions are selected as the elitism and delivered directly into the next iteration; (5) the rest of the electrode patterns are recombined by a two-point crossover method with a probability of 0.7 and mutated by inversion mutation method with a probability of 0.3; (6) the electrode patterns are filtered to avoid the checkboard phenomenon; and (7) update the electrode pattern for the next iteration until the algorithm is convergent, and the best electrode pattern is selected as the optimized result. The adjustment procedure of one electrode pattern during the optimization process is shown in Figure 4b. In the iterative optimization process for the single-point task, the result can be obtained with only 60 iterations. Time of each step in the iteration is only $1.9s$, which is related to the number of initial parameters set. Next, we take several experiments to prove the effectiveness of the algorithm.

Case I: Maximum displacement of a single point

Based on the above GA-based inverse design method, we first set the design object as maximum displacement of a single point toward an arbitrary direction. And the experimental setup is shown in Supplementary Fig. S7. Without loss of generality, the selected points and directions are illustrated in Supplementary Table S2. For the convenience of comparison, we also need eight intuitive designs (Fig. 5a). To construct the intuitive designs, we adopted a same rule for all cases instead of selecting specifical electrode pattern to deteriorate the output displacement of the intuitive design. We separate the dielectric elastomer membrane into two regions by a line that crosses the object point and is perpendicular to its desired motion direction, then the region behind the motion direction is selected as the electrode pattern. According to the above eight design objects, we separately employ the GA-based inverse design method by taking the coordinate and motion direction of the target point as an input to automatically design the electrode pattern. Based on the

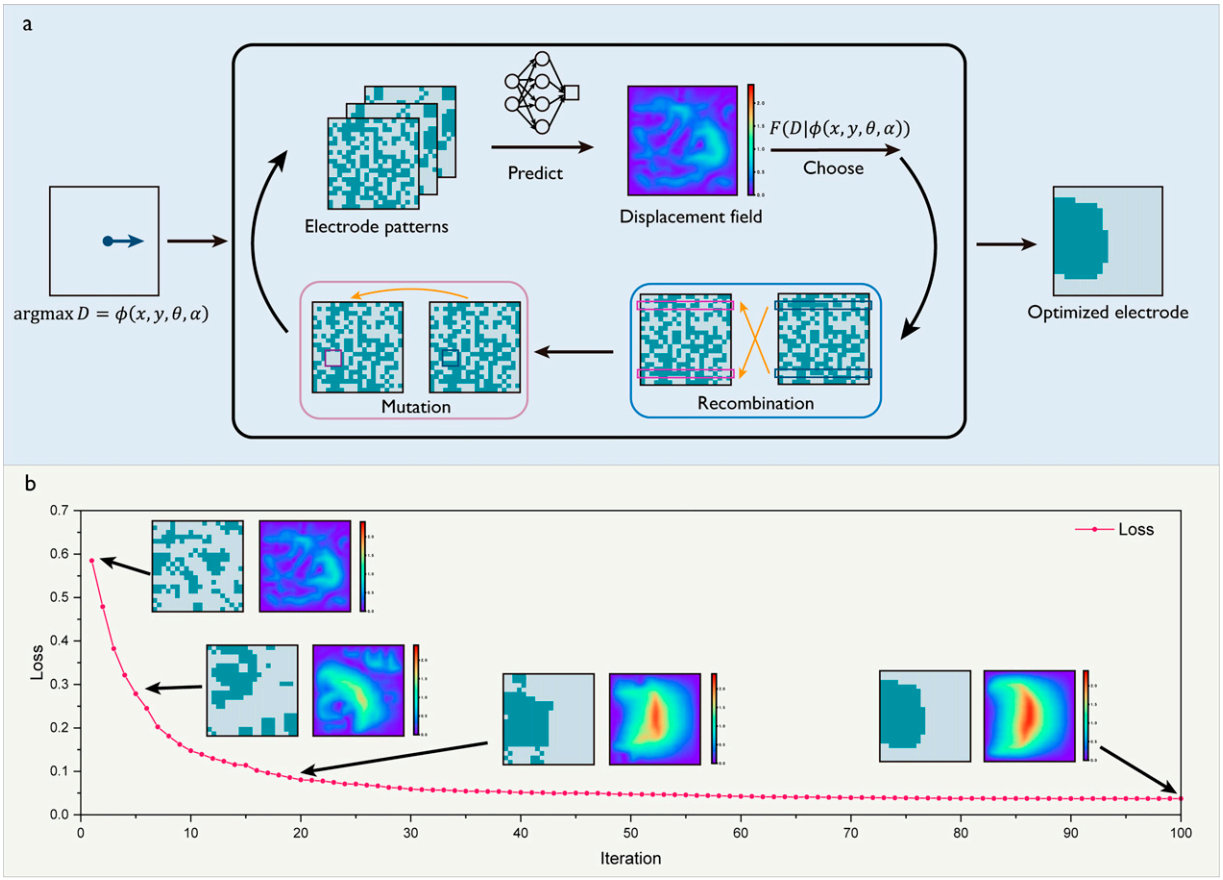

FIG. 4. Schematics of inverse design with genetic algorithm embedded neural network. **(a)** The procedures of GA, including the displacement field prediction and electrode pattern adjusting during one iteration. **(b)** The evolution of electrode pattern and the corresponding predicted displacement field on the loss curve during iterations.

designed electrode pattern, corresponding experiments are conducted and evaluated. Figure 5 and Supplementary Movie S2 show the design results, which demonstrate that:

1. For arbitrary points and directions, our method always can rapidly generate optimized electrode patterns (Fig. 5a), which will accelerate the application of DEAs in the field of soft robotics.
2. Compared with the intuitive design (Fig. 5b and Supplementary Fig. S8.), the performance of optimized electrode pattern is improved by about 30%, validating the effectiveness of our automatic design framework.

Case II: Maximum displacement under different area fraction

In the above analysis, we keep the area fraction of the electrode pattern constant. Of course, the area fraction also influences the performance of the planar DEAs. Therefore, changing area fraction is adopted to evaluate the expandability of the automatic design framework. To this end, the design object is selected as maximum displacement of the central point under different area fraction, which can be described as:

$$\arg\max D = \phi(100, 100, 0, \alpha) \tag{7}$$

Based on the above design object, the area fraction is changing from 5% to 95% by a step of 5%. Then, our GA-based inverse design method is adopted to optimize the electrode pattern under different area fraction. Figure 5a shows the optimization results. It can be observed that: as the area fraction increases, the maximum displacement of the central point increases first and then decreases. This phenomenon matches with our experience: for the planar DEA, too large or too small area fraction will hinder the deformation of the dielectric elastomer membrane. In addition, it also demonstrates that although our surrogate model is trained based on a constant area fraction of electrode pattern, our design framework can also self-adapt different area fraction.

Case III: Maximum displacement of multiple points

Except the single point, we further explore the application for motion of multiple points. To this end, we select two kinds of design objects. The first one is to design an electrode pattern that simultaneously generates the centripetal motion of four points. The second one is to simultaneously generate the rotation motion of four points. Two design objects can be expressed as:

$$\arg\max D_i = \sum_i \phi(x_i, y_i, \theta_i) \tag{8}$$

Based on the above deign objects, we adopt the automatic design framework to design the electrode patterns. Figure 6b and Supplementary Fig. S9 show the simulation results and

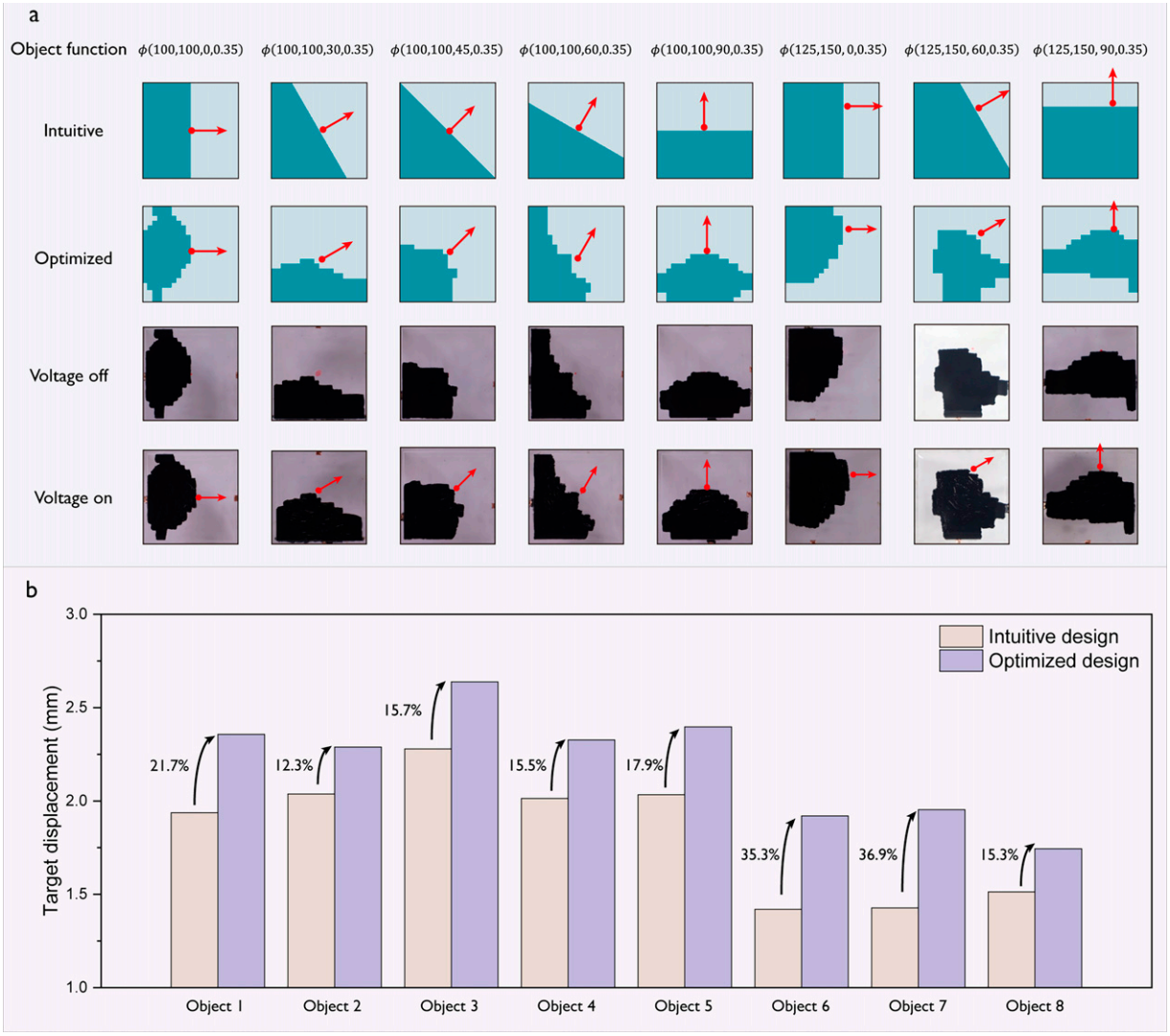

FIG. 5. Designed DEAs of maximum displacement of a single point. **(a)** The comparison of optimized electrode patterns and the intuitive one. **(b)** Experimental results of maximum displacement of target points.

experimental data. It can be seen that with the optimized electrode pattern, the four points can generate centripetal motion with 0.8 mm and the rotation motion by 2°, validating the effectiveness of our automatic design framework for complex design objects (Supplementary Movie S2).

Case IV: Multiple solutions

Due to the high-dimensional design space, multiple solutions may widely exist for the same design object. By taking advantage of the GA, it can easily generate multiple solutions. As shown in Figure 6c, we employ our automatic design framework to generate eight electrode patterns with basically same maximum displacement of the central point (about 2.2 mm). Furthermore, when the displacement of the central point is set as 1.0 mm, our automatic design framework also can generate a series of electrode patterns (such as the eight electrode patterns shown in Fig. 6d) with different shape and area fraction. The capability of multiple solutions of our automatic design framework may contribute to satisfying different application conditions of DEAs.

Conclusions

In this work, we propose a deep learning-based design framework for DEAs to automatically generate distributed electrode patterns based on desired performances. To this end, we first establish a membrane element through UMAT in ABAQUS to generate dataset for training neural network and propose a dataset construction approach to optimize the distribution of the dataset. With the optimized dataset, a neural network-embedded physical information is trained to accurately and rapidly predict continuous deformation under arbitrary electrode patterns within 0.011*s*. Finally, by using the neural network as a surrogate model, a GA is introduced to automatically design the electrode pattern of DEAs. To validate the automatic design framework, various design objects (including maximum displacement, multiple object optimization, multiple solutions, and complex actuations) are adopted. Both simulation data and experimental results demonstrate that our automatic design framework can rapidly design the electrode pattern within 2 min with obviously improved performance. In addition, our design framework is capable of

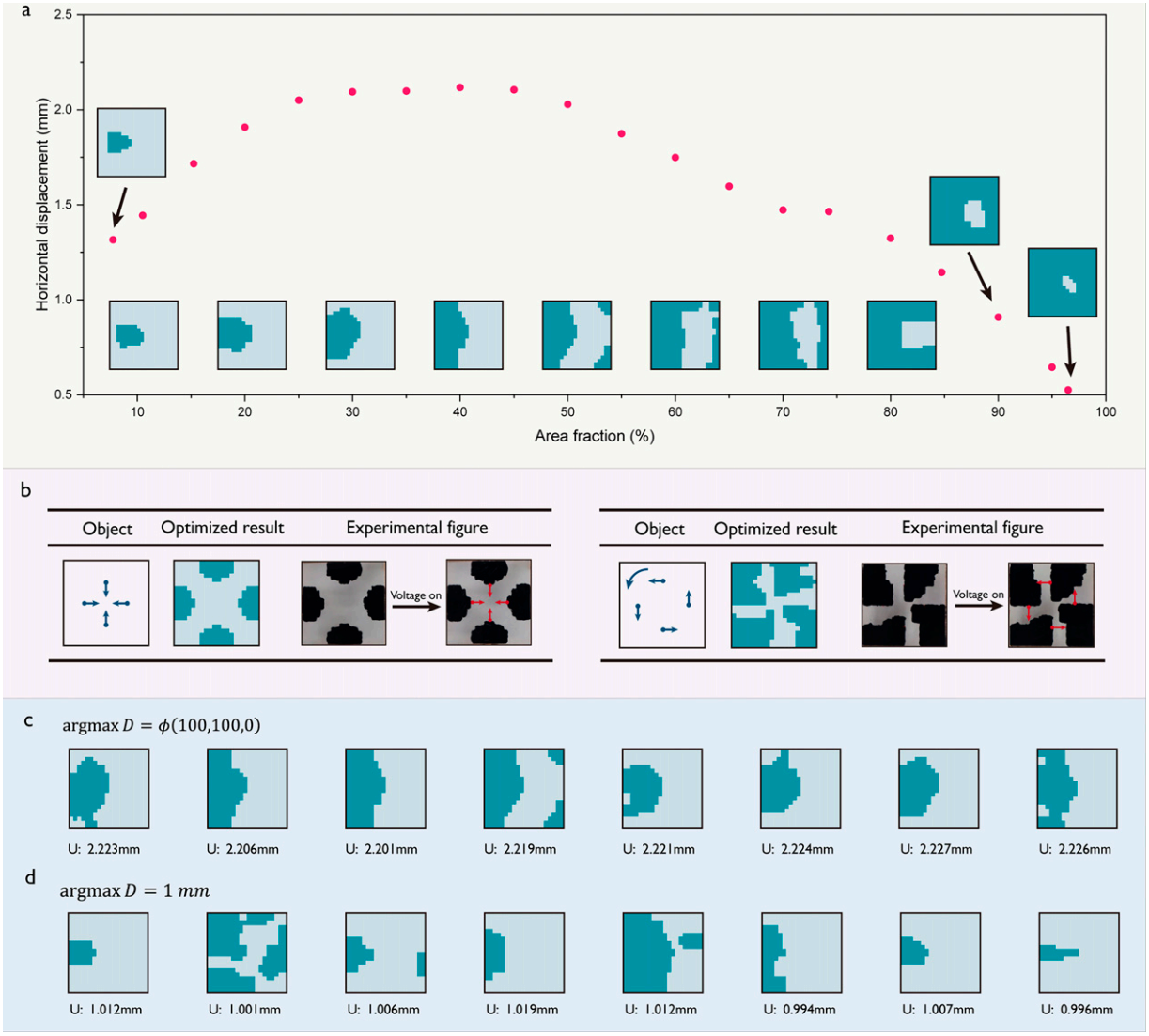

FIG. 6. Experimental results of multiple tasks. **(a)** Optimization results of the maximum displacement of center point under different area fraction constraints. **(b)** Optimization results of maximum displacement of multiple points. **(c)** Multiple solutions of maximum displacement of the center point. **(d)** Multiple solutions of electrode pattern at a certain displacement 1.00 mm.

generating multiple solutions and beyond expectation electrode patterns, which may contribute to broaden the applications of DEAs. With the fast and automatic design framework, we can improve the performance of DEAs for propelling their applications in soft robots. In the future, we would like to consider the viscoelasticity of the materials in the FEM and extend the automatic optimization framework to fit the design demands with dynamical response of DEAs. Nevertheless, our framework contributes to rapidly and automatically design DEAs with high performance and high-dimensional design spaces, accelerating the practical applications of DEAs.

Acknowledgment

The authors thank openbayes.com for providing high-performance computing.

Author Disclosure Statement

No competing financial interests exist.

Funding Information

This work was supported in part by the National Natural Science Foundation of China under Grant 52275024 and 52025057, in part by the Natural Science Foundation of Shanghai under Grant 23ZR1435500, and in part by the Chenguang Program of Shanghai Education Development Foundation and Shanghai Municipal Education Commission under Grant 22CGA11.

Supplementary Material

Supplementary Table S1
Supplementary Table S2
Supplementary Movie S1
Supplementary Movie S2
Supplementary Data S1
Supplementary Data S2
Supplementary Figure S1
Supplementary Figure S2

Supplementary Figure S3
Supplementary Figure S4
Supplementary Figure S5
Supplementary Figure S6
Supplementary Figure S7
Supplementary Figure S8
Supplementary Figure S9

Reference

1. Zhang L, Huang X, Cole T, et al. 3D-printed liquid metal polymer composites as NIR-responsive 4D printing soft robot. Nat Commun 2023;14(1):7815; doi: 10.1038/s41467-023-43667-4
2. Jin B, Song H, Jiang R, et al. Programming a crystalline shape memory polymer network with thermo- and photo-reversible bonds toward a single-component soft robot. Sci Adv 2018;4(1):eaao3865; doi: 10.1126/sciadv.aao3865
3. Ze Q, Kuang X, Wu S, et al. Magnetic shape memory polymers with integrated multifunctional shape manipulation. Adv Mater 2020;32(4):e1906657; doi: 10.1002/adma.201906657
4. Xia Y, He Y, Zhang F, et al. A review of shape memory polymers and composites: Mechanisms, materials, and applications. Adv Mater 2021;33(6):e2000713; doi: 10.1002/adma.202000713
5. Liu H, Tian H, Li X, et al. Shape-programmable, deformation-locking, and self-sensing artificial muscle based on liquid crystal elastomer and low–melting point alloy. Sci Adv 2022;8(20):eabn5722; doi: 10.1126/sciadv.abn5722
6. Kim D, Kim B, Shin B, et al. Actuating compact wearable augmented reality devices by multifunctional artificial muscle. Nat Commun 2022;13(1):4155; doi: 10.1038/s41467-022-31893-1
7. Feng M, Yang D, Majidi C, et al. High-speed and low-energy actuation for pneumatic soft robots with internal exhaust air recirculation. Adv Intell Syst 2023;5(4):2200257; doi: 10.1002/aisy.202200257
8. Feng M, Yang D, Ren L, et al. X-crossing pneumatic artificial muscles. Sci Adv 2023;9(38):eadi7133; doi: 10.1126/sciadv.adi7133
9. Mirvakili SM, Sim D, Hunter IW, et al. Actuation of untethered pneumatic artificial muscles and soft robots using magnetically induced liquid-to-gas phase transitions. Sci Robot 2020;5(41):eaaz4239; doi: 10.1126/scirobotics.aaz4239
10. Higueras-Ruiz DR, Shafer MW, Feigenbaum HP. Cavatappi artificial muscles from drawing, twisting, and coiling polymer tubes. Sci Robot 2021;6(53):eabd5383; doi: 10.1126/scirobotics.abd5383
11. Li S, Vogt DM, Rus D, et al. Fluid-driven origami-inspired artificial muscles. Proc Natl Acad Sci U S A 2017;114(50):13132–13137; doi: 10.1073/pnas.1713450114
12. Pelrine RE, Kornbluh RD, Joseph JP. Electrostriction of polymer dielectrics with compliant electrodes as a means of actuation. Sens Actuators Phys 1998;64(1):77–85; doi: 10.1016/S0924-4247(97)01657-9
13. Pelrine R, Kornbluh R, Pei Q, et al. High-speed electrically actuated elastomers with strain greater than 100%. Science 2000;287(5454):836–839; doi: 10.1126/science.287.5454.836
14. Lochmatter P, Michel SA, Kovacs GM. Electromechanical model for static and dynamic activation of elementary dielectric elastomer actuators. In: Smart Structures and Materials 2006: Electroactive Polymer Actuators and Devices (EAPAD). SPIE; 2006, pp. 105–117; doi: 10.1117/12.657873
15. Zhao H, Hussain AM, Duduta M, et al. Compact dielectric elastomer linear actuators. Adv Funct Materials 2018;28(42):1804328; doi: 10.1002/adfm.201804328
16. Xu L, Chen H-Q, Zou J, et al. Bio-inspired annelid robot: A dielectric elastomer actuated soft robot. Bioinspir Biomim 2017;12(2):e025003; doi: 10.1088/1748-3190/aa50a5
17. Tang C, Du B, Jiang S, et al. A pipeline inspection robot for navigating tubular environments in the sub-centimeter scale. Sci Robot 2022;7(66):eabm8597; doi: 10.1126/scirobotics.abm8597
18. Lu X, Wang K, Hu T. Development of an annelid-like peristaltic crawling soft robot using dielectric elastomer actuators. Bioinspir Biomim 2020;15(4):e046012; doi: 10.1088/1748-3190/ab8af6
19. Li J, Liu L, Liu Y, et al. Dielectric elastomer spring-roll bending actuators: Applications in soft robotics and design. Soft Robot 2019;6(1):69–81; doi: 10.1089/soro.2018.0037
20. Baltes M, Kunze J, Prechtl J, et al. A bi-stable soft robotic bendable module driven by silicone dielectric elastomer actuators: Design, characterization, and parameter study. Smart Mater Struct 2022;31(11):114002; doi: 10.1088/1361-665X/ac96df
21. Lee S, Moghani M, Li A, et al. A small steerable tip based on dielectric elastomer actuators. IEEE Robot Autom Lett 2023;8(10):6531–6538; doi: 10.1109/LRA.2023.3308335
22. Zhang C, Zhang C, Qu J, et al. Underwater and surface aquatic locomotion of soft biomimetic robot based on bending rolled dielectric elastomer actuators. In: 2023 IEEE/RSJ International Conference on Intelligent Robots and Systems (IROS). 2023, pp. 4677–4682; doi: 10.1109/IROS55552.2023.10342144
23. Wang S, Chen Z. Modeling of two-dimensionally maneuverable jellyfish-inspired robot enabled by multiple soft actuators. IEEE/ASME Trans Mechatron 2022;27(4):1998–2006; doi: 10.1109/TMECH.2022.3172434
24. Koenigsdorff M, Mersch J, Pfeil S, et al. High-strain helical dielectric elastomer actuators. In: Electroactive Polymer Actuators and Devices (EAPAD) XXIV. SPIE; 2022; pp. 149–159; doi: 10.1117/12.2612172
25. Chen Y, Zhao H, Mao J, et al. Controlled flight of a microrobot powered by soft artificial muscles. Nature 2019;575(7782):324–329; doi: 10.1038/s41586-019-1737-7
26. Chen Y, Xu S, Ren Z, et al. Collision resilient insect-scale soft-actuated aerial robots with high agility. IEEE Trans Robot 2021;37(5):1752–1764; doi: 10.1109/TRO.2021.3053647
27. Ren Z, Kim S, Ji X, et al. A high-lift micro-aerial-robot powered by low-voltage and long-endurance dielectric elastomer actuators. Adv Mater 2022;34(7):e2106757; doi: 10.1002/adma.202106757
28. Li G, Chen X, Zhou F, et al. Self-powered soft robot in the Mariana Trench. Nature 2021;591(7848):66–71; doi: 10.1038/s41586-020-03153-z
29. Zhang Y, Ding M, Zhu S, et al. Conceptual design and simulation of a BCF swimming soft robotic fish for deep-sea. In: 2022 IEEE International Conference on Robotics and Biomimetics (ROBIO). 2022; pp. 111–115; doi: 10.1109/ROBIO55434.2022.10012026
30. Sriratanasak N, Axinte D, Dong X, et al. Tasering twin soft robot: A multimodal soft robot capable of passive flight and wall climbing. Adv Intell Syst 2022;4(12):2200223; doi: 10.1002/aisy.202200223
31. Hu T, Lu X, Liu J. Inchworm-like soft robot with multimodal locomotion using an acrylic stick-constrained dielectric

elastomer actuator. Adv Intell Syst 2023;5(2):2200209; doi: 10.1002/aisy.202200209
32. Gu G, Zou J, Zhao R, et al. Soft wall-climbing robots. Sci Robot 2018;3(25):eaat2874; doi: 10.1126/scirobotics.aat2874
33. Jiang S, Tang C, Dong X, et al. Soft pocket pump for multi-medium transportation via an active tubular diaphragm. Adv Funct Materials 2023;33(50):2305289; doi: 10.1002/adfm.202305289
34. Zhao H, Hussain AM, Israr A, et al. A wearable soft haptic communicator based on dielectric elastomer actuators. Soft Robot 2020;7(4):451–461; doi: 10.1089/soro.2019.0113
35. Lee D-Y, Jeong SH, Cohen AJ, et al. A wearable textile-embedded dielectric elastomer actuator haptic display. Soft Robot 2022;9(6):1186–1197; doi: 10.1089/soro.2021.0098
36. Ji X, Liu X, Cacucciolo V, et al. Untethered feel-through haptics using 18-μm thick dielectric elastomer actuators. Adv Funct Mater 2021;31(39):2006639; doi: 10.1002/adfm.202006639
37. Leroy E, Hinchet R, Shea H. Multimode hydraulically amplified electrostatic actuators for wearable haptics. Adv Mater 2020;32(36):e2002564; doi: 10.1002/adma.202002564
38. Zhou J, Hong W, Zhao X, et al. Propagation of instability in dielectric elastomers. Int J Solids Struct 2008;45(13):3739–3750; doi: 10.1016/j.ijsolstr.2007.09.031
39. Park HS, Wang Q, Zhao X, et al. Electromechanical instability on dielectric polymer surface: Modeling and experiment. Comput Methods Appl Mech Eng 2013;260:40–49; doi: 10.1016/j.cma.2013.03.020
40. Henann DL, Chester SA, Bertoldi K. Modeling of dielectric elastomers: Design of actuators and energy harvesting devices. J Mech Phys Solids 2013;61(10):2047–2066; doi: 10.1016/j.jmps.2013.05.003
41. Zhang Z-Q, Foo CC, Liu GR. A semi-explicit finite element method for dynamic analysis of dielectric elastomers. Int J Comput Methods 2015;12(01):1350108; doi: 10.1142/S0219876213501089
42. Liu J, Foo CC, Zhang Z-Q. A 3D multi-field element for simulating the electromechanical coupling behavior of dielectric elastomers. Acta Mech Solida Sin 2017;30(4):374–389; doi: 10.1016/j.camss.2017.07.005
43. Anonymous. Mechanics of dielectric elastomer structures: A review. Extreme Mech Lett 2020;38:100752; doi: 10.1016/j.eml.2020.100752
44. Wang N, Guo H, Chen B, et al. Design of a rotary dielectric elastomer actuator using a topology optimization method based on pairs of curves. Smart Mater Struct 2018;27(5):e055011; doi: 10.1088/1361-665X/aab991
45. Chen B, Wang N, Wang R, et al. Automatic design of dielectric elastomer-based crawling robots using shape and topology optimization. J Mech Robot 2023;15(2); doi: 10.1115/1.4054642
46. Wang N, Guo H, Chen B, et al. Integrated design of actuation and mechanism of dielectric elastomers using topology optimization based on fat Bezier curves. Soft Robot 2019;6(5):644–656; doi: 10.1089/soro.2018.0114
47. Wang N, Guo H, Chen B, et al. Design of dielectric elastomer actuator using topology optimization method based on genetic algorithm. Smart Mater Struct 2019;28(6):e065013; doi: 10.1088/1361-665X/ab15c6
48. Chen FF, Liu K, Wang YQ, et al. Automatic design of soft dielectric elastomer actuators with optimal spatial electric fields. IEEE Trans Robot 2019;35(5):1150–1165; doi: 10.1109/Tro.2019.2920108
49. Chen B, Wang N, Zhang X, et al. Design of dielectric elastomer actuators using topology optimization on electrodes. Smart Mater Struct 2020;29(7):e075029; doi: 10.1088/1361-665X/ab8b2d
50. Yang C, Kim Y, Ryu S, et al. Prediction of composite microstructure stress-strain curves using convolutional neural networks. Mater Des 2020;189:108509; doi: 10.1016/j.matdes.2020.108509
51. Qin C, Shi G, Tao J, et al. Precise cutterhead torque prediction for shield tunneling machines using a novel hybrid deep neural network. Mech Syst Signal Process 2021;151:107386; doi: 10.1016/j.ymssp.2020.107386
52. Zheng X, Zhang X, Chen T-T, et al. Deep learning in mechanical metamaterials: From prediction and generation to inverse design. Adv Mater 2023;35(45):e2302530; doi: 10.1002/adma.202302530
53. Almasri W, Bettebghor D, Ababsa F, et al. Deep learning architecture for topological optimized mechanical design generation with complex shape criterion. In: Advances and Trends in Artificial Intelligence. Artificial Intelligence Practices. (Fujita H, Selamat A, Lin JC-W, et al. eds). Springer International Publishing: Cham; 2021; pp. 222–234; doi: 10.1007/978-3-030-79457-6_19
54. Mater AC, Coote ML. Deep learning in chemistry. J Chem Inf Model 2019;59(6):2545–2559; doi: 10.1021/acs.jcim.9b00266
55. Atz K, Grisoni F, Schneider G. Geometric deep learning on molecular representations. Nat Mach Intell 2021;3(12):1023–1032; doi: 10.1038/s42256-021-00418-8
56. Mosser L, Barbé L, Rubbert L, et al. Towards automatic design of soft pneumatic actuators: Inner structure design using CNN model and Bézier curve-based genetic algorithm. IEEE Robot Autom Lett 2023;8(10):6603–6610; doi: 10.1109/LRA.2023.3309135
57. Li Y, Liu J, Liang W, et al. Towards optimal design of dielectric elastomer actuators using a graph neural network encoder. IEEE Robot Autom Lett 2023;8(10):6339–6346; doi: 10.1109/LRA.2023.3306647
58. Forte AE, Hanakata PZ, Jin LS, et al. Inverse design of inflatable soft membranes through machine learning. Adv Funct Materials 2022;32(16); doi: 10.1002/adfm.202111610

Address correspondence to:
Jiang Zou
State Key Laboratory of Mechanical System and Vibration
Shanghai Jiao Tong University
Shanghai 200240
China

E-mail: zoujiang@sjtu.edu.cn

Guoying Gu
State Key Laboratory of Mechanical System and Vibration
Shanghai Jiao Tong University
Shanghai 200240
China

E-mail: guguoying@sjtu.edu.cn